

# Prospects for Detecting Dark Matter Halo Substructure with Pulsar Timing

Shant Baghran,<sup>1,\*</sup> Niayesh Afshordi,<sup>2,3</sup> and Kathryn M. Zurek<sup>4</sup>

<sup>1</sup>*Department of Physics, Sharif University of Technology, P.O.Box 11365-9161, Tehran, Iran*

<sup>2</sup>*Perimeter Institute for Theoretical Physics, 31 Caroline St. N., Waterloo, ON, N2L 2Y5, Canada*

<sup>3</sup>*Department of Physics and Astronomy, University of Waterloo,  
200 University Avenue West, Waterloo, ON, N2L 3G1, Canada*

<sup>4</sup>*Michigan Center for Theoretical Physics, Department of Physics,  
University of Michigan, Ann Arbor, MI 48109, USA*

One of the open questions of modern cosmology is the nature and properties of the Dark Matter halo and its substructures. In this work we study the gravitational effect of dark matter substructures on pulsar timing observations. Since millisecond pulsars are stable and accurate emitters, they have been proposed as plausible astrophysical tools to probe the gravitational effects of dark matter structures. We study this effect on pulsar timing through Shapiro time delay (or Integrated Sachs-Wolfe (ISW) effect) and Doppler effects statistically, showing that the latter dominates the signal. For this task, we relate the power spectrum of pulsar frequency change to the matter power spectrum on small scales, which we compute using the stable clustering hypothesis. We compare this power spectrum with the reach of current and future observations of pulsar timing designed for gravitational wave (GW) detection. Our results show that while current observations are unable to detect these signals, the sensitivity of the upcoming Square Kilometer Array (SKA) is only a factor of few weaker than our optimistic predictions.

PACS numbers: 04.50.+h, 95.36.+x, 98.80.-k

## I. INTRODUCTION

One of the greatest puzzles of modern cosmology is the nature of the Dark Matter (DM). The latest cosmological observations indicate that DM has a mean cosmic mass density  $\sim 5$  times larger than the density of the baryonic matter (*e.g.* see WMAP-7 year results [1]), and its presence is confirmed by a large amount of astrophysical evidence, such as rotation curves of galaxies, gravitational lensing effects, growth of large scale structure of the Universe, big bang nucleosynthesis and the dynamics of the Universe as a whole [2]. The cosmological and astrophysical observations that may lead us to better understand this unknown component of the Universe are areas of intense study, focusing on DM's nature as particles, its structure, distribution and effect on the other components of the Universe. Studying the small scale structure of DM, for example, will tell us something about the DM particle's fundamental properties. Consequently, finding new footprints of DM in astrophysical observations is important for opening new horizons in DM studies.

The theory of structure formation, which is based on gravitational instability of primordial matter density fluctuations and the hierarchical scheme of structure formation, assumes that collisionless DM is the main in-

gredient in today's cosmological structures. One of the features of this theory is that DM collapses into bound states, known as DM halos. A cold dark matter primordial power spectrum predicts a large range of mass scales for these DM halos, from  $10^{12} - 10^{14} M_{\odot}$  down to  $10^{-12} - 10^{-4} M_{\odot}$  [3]. Larger halos form from merger of smaller halos which may partly survive as substructure of bigger halos.

The statistics of DM distribution and the dynamics of this substructure may have an effect on astrophysical observations. One of the promising astrophysical probes for studying the distribution of interstellar medium (ISM) which is considered to be mostly baryonic matter are pulsars [4]. ISM causes a dispersion on pulsars' light which in turn has an effect on pulsar timing residuals.

In the present work, we push this one step further and study the *gravitational effects* of dark matter halo substructure on pulsar timing. This effect manifests itself through the 1) Shapiro time delay effect [5], and 2) Doppler effect. The Shapiro time delay is caused by the presence of dark matter's dynamical potential along the line of sight. On the other hand, the Doppler effect is caused by the acceleration of the observer/pulsar because of the pull of DM subhalos. Probing dark matter substructure by Shapiro time delay in pulsar timing was first proposed by Siegel *et al.* by considering the effect of one DM subhalo crossing the line of sight [6]. The Shapiro delay of low frequency pulsars in globular clusters was also studied in [7]. Recently, the effect of DM subha-

---

\*Electronic address: baghran@physics.sharif.edu

los crossing the line of sight was studied in astrometric microlensing [8].

In this work, as a complementary and more realistic view, we consider the statistical distribution of DM substructure and its effect on pulsars' timing residual. In order to study the effect of the DM substructure distribution on pulsar timing, we need a structure formation model. On very small scales deep into the nonlinear regime of structure formation, which is unaffected by halo merging or tidal disruption, we can use the stable clustering hypothesis. The stable clustering hypothesis was first introduced by Davis & Peebles [9] as an analytic technique to study the galaxy correlation function in the deeply nonlinear regime, and was subsequently applied to fitting formulae for nonlinear correlation functions/power spectra [10, 11]. In the current work, we use the phase-space stable clustering model which was recently developed by Afshordi *et al.* [12].

The article is structured as follows. In Sec. (II), we first introduce millisecond pulsars. Then in the following subsections we derive the power spectrum of frequency change of pulsars for Shapiro time delay and Doppler effects. In Sec. (III), we review the stable clustering hypothesis in phase space. In Sec. (IV), we find the frequency change power spectrum and show its dependence on free parameters of the model, both for Shapiro and Doppler effects. In Sec. (V), we discuss the observational prospects of detecting these effects with current and future pulsar timing arrays. Finally, Sec. (VI) concludes the paper.

For reference, we set cosmological parameters to be  $\Omega_m^0 = 0.27$ ,  $\sigma_8 = 0.8$  and  $H_0 = 100h$  km/s/Mpc where  $h = 0.7$ .

## II. GRAVITATIONAL EFFECT ON POWER SPECTRUM OF PULSAR TIMING

In this section, we first introduce millisecond pulsars as promising astrophysical observational probes to detect the gravitational effects of DM substructures. Then we derive the statistics of frequency change due to Shapiro and Doppler effects.

### A. Millisecond Pulsars

The most stable, consistent astrophysical emitters in the known universe are millisecond pulsars, many of them remaining stable without flux change over timescales exceeding thirty years [13]. On account of this they have been used as precise tools to probe changes in the matter distribution between the pulsar and earth [14]. The pulsars with the highest rotational frequencies, and hence the shortest pulse to pulse periods, are the most stable with a time period of  $\mathcal{O}(1$  ms). The typical residual of

these pulsars is of order of  $\mathcal{O}(1 \mu\text{s})$ . This means that fluctuations in pulsar period within a short time scale (e.g.  $\sim 1$  hr) are less than  $\sim \mu\text{s}$ . These residuals do not accumulate, which means that the period remains constant during the time that a pulsar is stable. This is used to measure the pulsar's timing residuals with high accuracy during a long period ( $\sim 10$  years), and to search for non-intrinsic changes in pulsar timing. Consequently, to detect any physics besides the pulsars' intrinsic changes, we should search for a time delay larger than the intrinsic uncertainties. An important point is that many interesting non-intrinsic effects on pulsar timing will be correlated. An example is the attempt to detect gravitational waves through cross-correlation of pulsar timing arrays [15]. Another possible non-intrinsic effect which we consider in this work is the change of the gravitational potential. The transit of DM halo substructure across the line of sight, which causes the Shapiro delay, is studied in the following subsection. This discussion is followed by a consideration of the Doppler effect, caused by the acceleration of pulsar/observer due to presence of DM substructure.

### B. Shapiro time delay

The Shapiro time delay is caused by the presence of a time dependent gravitational potential along the line of sight. To quantify this effect, we can write the metric of perturbed space time as

$$ds^2 = -(1 + 2\Phi)dt^2 + (1 - 2\Phi)d\vec{x}^2, \quad (1)$$

where  $\Phi$  represents the Newtonian potential in the weak field limit and we set the speed of light  $c = 1$ . In the case of pulsars, we can write the null geodesics for a pulse received at time  $t$  using the above metric as

$$t = t_0 + \delta t = \int_{x_{em}}^{x_{obs}} (1 - 2\Phi)d\vec{x}, \quad (2)$$

where  $\delta t$  is obtained from integration over the perturbed potential along the line of sight. As it is not possible to measure the absolute light travel time of any astrophysical object, we need to observe the time arrival changes over a detection period. The time derivative of the pulsar time residual is defined as

$$\dot{\delta t} = -\frac{\delta\nu}{\nu} = -2 \int \dot{\Phi} d\vec{x}, \quad (3)$$

where  $\nu$  is the frequency of the pulsar, and  $\delta\nu$  is the change in frequency (we note that this is identical to the cosmological Integrated Sachs-Wolfe (ISW) effect [16]). In order to find a statistical description of the induced time delays, we assume that DM substructures move with a constant velocity  $v$  across the line of sight in the  $x$ -direction. We refer to this as the *moving screen* approximation, which enables us to relate the time derivatives to

the spatial gradients of metric, *i.e.*  $\dot{\Phi} = v \frac{\partial}{\partial x} \Phi$ . The temporal correlation of the frequency changes is then given by

$$\langle (\frac{\delta\nu}{\nu})_1 (\frac{\delta\nu}{\nu})_n \rangle = 4 \int_0^{z_0} \int_0^{z_0} dz_1 dz_n v^2 \langle \frac{\partial}{\partial x} \Phi_1 \frac{\partial}{\partial x} \Phi_n \rangle, \quad (4)$$

where  $z_0$  is the position of the pulsar in the  $z$ -direction (line of sight), which we take to be  $\sim 1$  kpc, and  $\Phi_1$  and  $\Phi_n$  correspond to potentials at two different times. Now we can express the right hand side of Eq. (4) in Fourier space as:

$$\langle (\frac{\delta\nu}{\nu})_1 (\frac{\delta\nu}{\nu})_n \rangle = 4v^2 \int_0^{z_0} \int_0^{z_0} dz_1 dz_n \int \frac{d^3 \vec{k}_1}{(2\pi)^3} \int \frac{d^3 \vec{k}_n}{(2\pi)^3} (i\vec{k}_1^x)(i\vec{k}_n^x) \langle \Phi(\vec{k}_1) \Phi(\vec{k}_n) \rangle e^{-i\vec{k}_1 \cdot \vec{r}_1} e^{-i\vec{k}_n \cdot \vec{r}_n}. \quad (5)$$

By integrating over  $z_1$  and  $z_n$ , and using the definition of the potential power spectrum,

$$\langle \Phi(\vec{k}_1) \Phi(\vec{k}_n) \rangle = (2\pi)^3 \delta^3(\vec{k}_1 + \vec{k}_n) P_\Phi(\vec{k}), \quad (6)$$

Eq. (5) becomes

$$\langle (\frac{\delta\nu}{\nu})_1 (\frac{\delta\nu}{\nu})_n \rangle = 4v^2 \int \frac{d^3 \vec{k}_1}{(2\pi)^3} \left[ k_1^x z_0 \text{sinc}\left(\frac{k_1^x z_0}{2}\right) \right]^2 \times P_\Phi(\vec{k}_1) e^{-i\vec{k}_1^x (x_1 - x_n)}, \quad (7)$$

where  $\text{sinc}(x) \equiv \frac{\sin(x)}{x}$ . We can take the integral over  $k^z$ , which results in

$$\langle (\frac{\delta\nu}{\nu})_1 (\frac{\delta\nu}{\nu})_n \rangle = 4z_0 v^2 \int \int \frac{dk_y}{2\pi} \frac{dk_x}{2\pi} P_\Phi(\vec{k}) \times (k_x)^2 e^{-i\vec{k}^x v(t_1 - t_2)}, \quad (8)$$

where we omit the subscript 1 and replace  $x_1 = vt_1$  in the moving screen approximation (we also assume  $k_z \sim z_0^{-1} \ll k_x, k_y$ ). Now by considering the definition of the time-delay power spectrum,

$$\langle (\frac{\delta\nu}{\nu})_1 (\frac{\delta\nu}{\nu})_n \rangle = \frac{1}{2\pi} \int P_{\frac{\delta\nu}{\nu}}(\omega) e^{-i\omega \Delta t} d\omega, \quad (9)$$

we can integrate Eq. (8) over the time difference of two observations to obtain the power spectrum,

$$P_{\frac{\delta\nu}{\nu}}(\omega) = \int \langle (\frac{\delta\nu}{\nu})_1 (\frac{\delta\nu}{\nu})_n \rangle e^{i\omega \Delta t} d(\Delta t) = \int d(\Delta t) 4z_0 v^2 \int \int \frac{dk_y}{2\pi} \frac{dk_x}{2\pi} P_\Phi(\vec{k}) (k_x)^2 e^{-i\vec{k}^x v(\Delta t)} e^{i\omega \Delta t}, \quad (10)$$

where  $\Delta t = t_1 - t_2$ . Now the integration over  $dk_x$  and  $d(\Delta t)$  gives us the relation between  $k_x$  and the frequency as  $k_x v = \omega$ . Consequently Eq. (10) simplifies to:

$$\omega P_{\frac{\delta\nu}{\nu}}(\omega) = \frac{4z_0}{v} \int \frac{dk_y}{2\pi} \omega^3 P_\Phi \left( \sqrt{\frac{\omega^2}{v^2} + k_y^2} \right) \quad (11)$$

Using the Poisson equation, we can relate the potential power spectrum to the matter power spectrum  $P_\rho(\vec{k})$ :

$$P_\Phi(\vec{k}) = \left( \frac{4\pi G}{k^2} \right)^2 P_\rho(\vec{k}). \quad (12)$$

Finally by inserting Eq. (12) in Eq. (11), we find the dimensionless  $\omega P(\omega)$  in terms of the matter power spectrum:

$$\omega P_{\frac{\delta\nu}{\nu}}(\omega)|_{\text{Shapiro}} = \frac{4z_0}{v} \int \frac{dk_y}{2\pi} \omega^3 \left( \frac{4\pi G}{k^2} \right)^2 \bar{\rho}^2 P_{NL} \left( \sqrt{\frac{\omega^2}{v^2} + k_y^2} \right), \quad (13)$$

where we replace  $P_\rho(\vec{k}) = \bar{\rho}^2 P_{NL}(\vec{k})$ , in which  $\bar{\rho}$  is the mean cosmic DM density. In Sec.(IV), we will derive this function by using the stable clustering hypothesis.

### C. Doppler effect

Changing the potential of DM substructure near pulsars or the earth will introduce a velocity shift, which affects pulsar frequencies via the Doppler effect. In the Doppler effect, the frequency change of a pulsar is related to the line of sight velocity as  $\frac{\delta\nu}{\nu} = v_{l.s.}$ . So the correlation of the frequency changes observed at two separate times  $t_1$  and  $t_2$  caused by the Doppler effect can be written as

$$\langle (\frac{\delta\nu}{\nu})_1 (\frac{\delta\nu}{\nu})_n \rangle = \int_{-\infty}^{t_1} dt \int_{-\infty}^{t_2} dt' \langle \nabla_z \Phi_1 \nabla_z \Phi_n \rangle \times e^{\varepsilon(t-t_1)} e^{\varepsilon(t'-t_2)}, \quad (14)$$

where  $\varepsilon$  is a small parameter to regulate the infrared divergence of the integral. Once more, we can write the right hand side of Eq. (14) in Fourier space. Integration over time variables with the limit of  $\varepsilon \rightarrow 0$  results in

$$\langle (\frac{\delta\nu}{\nu})_1 (\frac{\delta\nu}{\nu})_n \rangle = \int \frac{d^3 \vec{k}}{(2\pi)^3} P_\Phi(\vec{k}) \frac{(k_z)^2}{(k_x v)^2} e^{-i\vec{k}^x v(\Delta t)}, \quad (15)$$

where we used the moving screen approximation to replace time integrals by integrals over  $x$ . Again, using Eq. (9), we can write the power spectrum of frequency changes as

$$P_{\frac{\delta\nu}{\nu}}(\omega) = \int \langle (\frac{\delta\nu}{\nu})_1 (\frac{\delta\nu}{\nu})_n \rangle e^{i\omega \Delta t} d(\Delta t) = \int d(\Delta t) \int \frac{d^3 \vec{k}}{(2\pi)^3} P_\Phi(\vec{k}) \frac{(k_z)^2}{(k_x v)^2} e^{-i\vec{k}^x v(\Delta t)} e^{i\omega \Delta t}. \quad (16)$$

Integration over  $dk_x$  and  $d\Delta t$  gives us the relation between  $k_x$  and the frequency as  $\omega = k_x v$ . Consequently Eq. (16) results in

$$P_{\frac{\delta\nu}{\nu}}(\omega) = \frac{1}{v} \int \frac{dk_y}{2\pi} \int \frac{dk_z}{2\pi} \frac{k_z^2}{\omega^2} P_\Phi(\vec{k}). \quad (17)$$

Because of the symmetry between the integration over  $k_y$  and  $k_z$ , we can replace  $k_y^2$  by  $(k_y^2 + k_z^2)/2$  in Eq. (17), which leads to

$$P_{\delta\nu}(\omega) = \frac{1}{4\pi} \int dk_* \frac{k_*^3}{v\omega^2} P_\phi \left( \sqrt{\frac{\omega^2}{v^2} + k_*^2} \right), \quad (18)$$

where  $k_* = \sqrt{k_y^2 + k_z^2}$ . By using the Poisson equation, we can relate the potential power spectrum to matter power spectrum, and finally write the dimensionless power spectrum as

$$\omega P_{\delta\nu}(\omega)|_{\text{Doppler}} = \frac{1}{4\pi} \int dk_* \frac{k_*^3}{v\omega} \left( \frac{4\pi G}{k^2} \right)^2 \bar{\rho}^2 P_{NL} \left( \sqrt{\frac{\omega^2}{v^2} + k_*^2} \right). \quad (19)$$

As in the case of Shapiro delay, by knowing the matter power spectrum we can determine the pulsar timing power spectrum.

### III. STABLE CLUSTERING HYPOTHESIS

In this section, we discuss the stable clustering hypothesis as a model to describe the nonlinear structure formation that will give us the required matter power spectrum. We make use of the phase-space stable clustering model recently developed by Afshordi *et al.* [12]. The collisionless Boltzmann equation at the phase space coordinates,  $\vec{r} + \Delta\vec{r}$ ,  $\vec{v} + \Delta\vec{v}$  is approximately given by

$$\begin{aligned} \frac{df}{dt}(r + \Delta r, v + \Delta v, t) \simeq \\ \frac{\partial f}{\partial t} + \frac{\partial f}{\partial r} \cdot (v + \Delta v) - \frac{\partial f}{\partial v} \cdot [\nabla\Phi + (\Delta r \cdot \nabla)\nabla\Phi] = 0, \end{aligned} \quad (20)$$

where  $\Phi$  is the gravitational potential, and for simplicity we omit the vector signs of distances and velocities. We can re-express the above equation in terms of the phase space density in the comoving coordinates with particle  $i$ :

$$\tilde{f}_i(\Delta r, \Delta v) \equiv f(r_i + \Delta r, v_i + \Delta v). \quad (21)$$

Using this new function, we can write the Boltzmann Eq. (20) as

$$\frac{df}{dt} = \frac{\partial \tilde{f}_i}{\partial t} \Big|_{\Delta r, \Delta v} + \frac{\partial \tilde{f}_i}{\partial \Delta r} \cdot \Delta v - \frac{\partial \tilde{f}_i}{\partial \Delta v} \cdot (\Delta r \cdot \nabla) \nabla\Phi = 0. \quad (22)$$

Notice that Eq. (22) can be understood as the tidal limit of the Boltzmann equation in terms of the phase coordinates  $(\Delta r, \Delta v)$ , *i.e.* in the coordinate system comoving with particle  $i$ .

The stable clustering hypothesis assumes that  $\frac{\partial \tilde{f}_i}{\partial t} \Big|_{\Delta r, \Delta v}$  averaged over the particles vanishes for small  $\Delta r$  and  $\Delta v$ . This implies that the number of neighbors

Surfaces of constant phase space density in stable clustering hypothesis

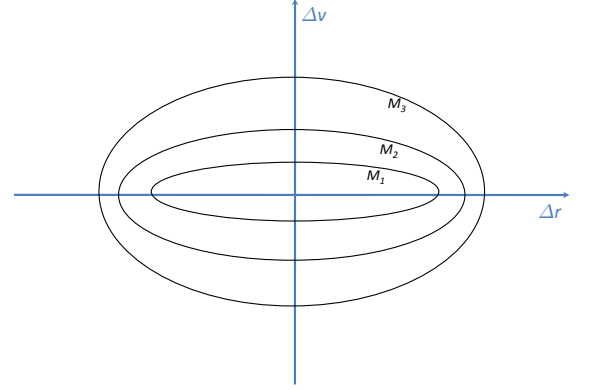


FIG. 1: Surfaces of constant average CDM phase space density,  $\langle \tilde{f} \rangle_p = \mu \xi_s$ , around a typical particle in the stable clustering hypothesis. The surfaces are assumed to be concentric ellipsoids (Eq. 24). The mass and Hubble scales at the collapse of the structure,  $M(\xi_s)$  and  $H(\xi_s)$ , are related to the phase space density,  $\mu \xi_s$ , on each surface via the spherical collapse results Eqs. (25-28), while  $\mu \sim 3\%$  is an empirical factor that quantifies tidal stripping and is fixed through comparison with numerical simulations [12].

within a fixed physical separation of a DM particle in the phase space does not vary with time. Now, if we assume that  $\langle \tilde{f}_i \nabla \nabla \Phi \rangle_p \approx \langle \tilde{f}_i \rangle_p \langle \nabla \nabla \Phi \rangle_p$ , then a solution to Eq. (22) is:

$$\langle \tilde{f} \rangle_p \equiv \frac{1}{N} \sum_i \tilde{f}_i = F[\Delta v^2 + \Delta x_j \Delta x_k \langle \partial_j \partial_k \Phi \rangle_p], \quad (23)$$

where  $F$  is the general solution with isotropic velocity distribution and  $N$  is the number of particles in the phase space volume of interest. By using the approximation of a spherically symmetric potential, the above solution can be re-written by applying the Poisson equation:

$$\langle \tilde{f} \rangle_p = \mu \xi_s = F[(\Delta v)^2 + 100 H^2(\xi_s) (\Delta r)^2], \quad (24)$$

where  $\xi_s$  and  $H(\xi_s)$  are the phase-space density and Hubble constant at the formation time of DM substructure, respectively (see Fig. 1). We also use the spherical collapse model prediction for the halo density, which is roughly 200 times the critical density at the formation time [17].  $\mu \simeq 3\%$  is the mean fraction of bound *particle pairs* that can survive the tidal disruption period, and is calibrated by comparison with N-body simulations [12]. To determine the function  $F$ , we use the spherical collapse model results. The phase-space density can be

expressed as

$$\xi_s \sim \frac{10H(\xi_s)}{G^2 M(\xi_s)}, \quad (25)$$

using the fact that the radius and velocity dispersion of halos are related as

$$\sigma_{vir} \sim 10Hr_{vir}. \quad (26)$$

The phase space volume of the collapsed halo, *i.e.* the volume of the constant- $\xi_s$  ellipsoid in Eq. (23), is  $M/\xi_s$ , and by using Eq. (25), we find

$$\left[ \frac{\pi F^{-1}(\mu\xi_s)}{10H(\xi_s)} \right]^3 = \frac{[GM(\xi_s)]^2}{10H(\xi_s)}. \quad (27)$$

Furthermore, the mass scale that collapses at a given cosmological epoch is characterized by

$$\left[ \frac{H(\xi_s)}{H_0} \right]^{-2/3} \sigma[M(\xi_s)] \sim \delta_c \simeq 1.7, \quad (28)$$

where  $\delta_c$  is the linear density threshold for the spherical collapse,  $\sigma[M]$  is the r.m.s top hat linear overdensity at the mass scale  $M$ , and  $H_0$  is the Hubble constant in the present epoch. Using the above result, the phase space correlation function is obtained as

$$\begin{aligned} & \langle f(r_1, v_1) f(r_2, v_2) \rangle \\ & \simeq \frac{1}{V_6} \int_{V_6} d^3r d^3v f(r, v) f(r + \Delta r, v + \Delta v) \\ & = \frac{1}{V_6} \sum_i f(r_i + \Delta r, v_i + \Delta v) = \frac{N}{V_6} \langle \tilde{f} \rangle_p \\ & \simeq \langle f(r_1, v_1) \rangle \langle f(r_2, v_2) \rangle + \mu \langle f(\bar{r}, \bar{v}) \rangle \xi_s(\Delta r, \Delta v). \end{aligned} \quad (29)$$

In the equation above we used the assumption of ergodicity to replace the ensemble average  $\langle \rangle$  by the volume average, in a given volume of phase space  $V_6$ , while  $(\bar{r}, \bar{v})$  are the mean values of  $(r_1, v_1)$  and  $(r_2, v_2)$ . The second term is based on the stable clustering described above, with the assumption that  $|\Delta v| = |v_1 - v_2| \ll \Delta v_{tid}$  and  $|\Delta r| = |r_1 - r_2| \ll \Delta r_{tid}$  where  $\Delta v_{tid}$  and  $\Delta r_{tid}$  characterize the tidal truncation radii in the phase space. On the other hand, the first term in Eq. (29) dominates for large separations in the phase space, where particles are not correlated. So Eq. (29) is an interpolation between the stable clustering and the smooth halo regimes. This is a crucial point in calculating the nonlinear power spectrum of structures on small scales where it is related to phase space density correlation  $\mu \langle f(\bar{r}, \bar{v}) \rangle \xi_s(\Delta r, \Delta v)$  term.

#### IV. PULSAR RESIDUAL POWER SPECTRUM FROM STABLE CLUSTERING HYPOTHESIS

In order to calculate the dimensionless power spectrum of pulsar frequency change, we need to know the power

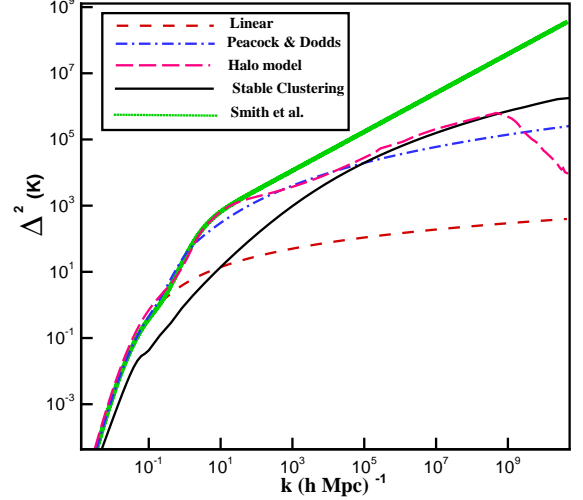


FIG. 2: Dimensionless power spectrum of density fluctuations  $\Delta^2(k) = \frac{k^3 P_{NL}(k)}{2\pi^2}$  as a function of wavenumber  $k$  for the linear regime (short-dashed line), Peacock and Dodds fitting formula (dash-dotted line), Smith et al. fitting formula (thick dotted line), halo model (long-dashed line) and for stable clustering hypothesis used in this work (solid line).

spectrum of matter on small scales. We now make use of the stable clustering hypothesis prediction, as developed in the previous section.

To use the stable clustering formula obtained in Eq. (29), we must relate the matter density power spectrum in Eqs. (13,19) to the real space correlation function of densities. In the stable clustering hypothesis in phase space, on small scales this relation becomes

$$\begin{aligned} \langle \rho(\vec{r}_1) \rho(\vec{r}_2) \rangle &= \int d^3\vec{v}_1 d^3\vec{v}_2 \langle f(\vec{r}_1, \vec{v}_1) f(\vec{r}_2, \vec{v}_2) \rangle \quad (30) \\ &\simeq \int d^3\vec{v} d^3\vec{v}' \Delta \vec{v} \mu \langle f(\vec{r}, \vec{v}) \rangle \xi_s(\Delta r, \Delta v) \\ &= \mu \bar{\rho}_{avg} \int d^3\vec{v} \xi_s(\Delta r, \Delta v). \end{aligned}$$

In order to find the dependance of the dimensionless power spectrum  $\omega P_{\delta\nu}(\omega)$  on  $\omega$ , we should have the r.m.s. top-hat linear overdensity  $\sigma(M)$ .  $\sigma(M)$  is the integral of linear matter power spectrum on a chosen window function as

$$\sigma^2(M) = \int \frac{d^3k}{(2\pi)^3} P_L(k) W^2(kR), \quad (31)$$

where  $P_L(k)$  and  $W(kR)$  are the linear matter power spectrum and the Fourier transform of the spherical top-hat filter of radius  $R$ , respectively, where

$$P_L(k) = Ak^{n_s} T^2(k), \quad (32)$$



$$W(x) = \frac{3(\sin x - x \cos x)}{x^3}. \quad (33)$$

Here  $n_s$  is the scalar spectral index of primordial matter power spectrum and  $M = 4\pi R^3 \bar{\rho}_m/3$ . The transfer function can be approximated by the BBKS [18] fitting formula,

$$T(k = q\Omega_m h^2 \text{Mpc}^{-1}) \approx \frac{\ln[1 + 2.34q]}{2.34q} \times [1 + 3.89q + (16.2q)^2 + (5.47q)^3 + (6.71q)^4]^{-1/4}. \quad (34)$$

Using Eqs. (30,31), and the stable clustering hypothesis, we can find an expression for the matter power spectrum on small scales, shown in Fig.(2) for a mass range  $10^{-6}$  to  $10^{12}$  solar masses and  $\mu = 0.03$ . For qualitative

comparison, we also plot the dimensionless power spectrum  $\Delta^2(k) = \frac{k^3}{2\pi^2} P_{NL}(k)$  obtained from the halo model of structure formation [19], as well as the fitting formulae of Peacock and Dodds [11] and Smith *et al.* for the nonlinear power spectrum [20]. We note that these approximations are based on fits to numerical simulations at  $k \lesssim 10^2 \text{Mpc}^{-1}$ , while the stable clustering hypothesis is expected to hold for  $k \gg 10 \text{Mpc}^{-1}$ , and thus should be a more appropriate measure of small scale dark matter structures. The cut-off in the halo model power spectrum is related to the size of smallest halo mass of  $M_{min} = 10^{-6} M_\odot$ .

Now, using the nonlinear power spectrum obtained from stable clustering, the dimensionless power spectrum for Shapiro time delay effect can be written as

$$\omega P_{\frac{\delta\nu}{\nu}}(\omega)|_{\text{Shapiro}} = \frac{4z_0}{v} \mu \bar{\rho}_{halo} \int \frac{dk_y}{2\pi} \omega^3 \frac{(4\pi G)^2}{k^4} \times \int 4\pi(\Delta r)^2 d(\Delta r) \frac{\sin(k\Delta r)}{k\Delta r} \int d(\Delta v) 4\pi(\Delta v)^2 \frac{10H[\xi_s(\Delta r, \Delta v)]}{G^2 M[\xi_s(\Delta r, \Delta v)]}. \quad (35)$$

In the case of the Doppler effect, we can also find the dimensionless power spectrum of pulsar frequency change in terms of phase space density derived from the stable clustering hypothesis. In this case Eq. (19) is expressed as

$$\omega P_{\frac{\delta\nu}{\nu}}(\omega)|_{\text{Doppler}} = \frac{\mu \bar{\rho}_{halo}}{v} \int \frac{dk_y}{4\pi} \frac{k_y^3}{\omega} \frac{(4\pi G)^2}{k^4} \times \int 4\pi(\Delta r)^2 d(\Delta r) \frac{\sin(k\Delta r)}{k\Delta r} \int d(\Delta v) 4\pi(\Delta v)^2 \frac{10H[\xi_s(\Delta r, \Delta v)]}{G^2 M[\xi_s(\Delta r, \Delta v)]}. \quad (36)$$

Notice that  $k = \sqrt{(\frac{\omega}{v})^2 + k_y^2}$ , and the Hubble parameter and the mass are related by  $\sigma(M)$  through Eq. (28).  $\bar{\rho}_{halo}$  is the smoothed halo local density at solar system which is assumed to be  $\sim 10^5 \rho_{crit}$ .

In order to numerically perform the 3d integrations in Eqs. (35-36) over  $(k_y, \Delta r, \Delta v)$ , we trade  $\Delta v$  with  $M$  as the integration variable using  $F^{-1} = (\Delta v)^2 + 100H^2(\Delta r)^2$  (see Fig. 1). We then perform the integration in three steps:

1. Noting that fixing  $M$  and  $\Delta r$  fixes  $\Delta v$  through Eqs. (24-28), we can first perform the  $k_y$  integral for fixed  $\Delta r$  and  $\Delta v$ . Since the integrand can have fast oscillations in  $k_y$ , we find asymptotic expansions for the  $k_y$  integral in the  $\omega\Delta r/v \gg$  and  $\ll 1$  limit, and devise an interpolation between the two regimes with less than 1% error, compared to the exact integral.
2. We then perform the  $\Delta r$  integral from zero to the maximum of  $(F^{-1})^{1/2}/(10H)$ , which is fixed by mass  $M$ , through Eq. (24).
3. Finally, we take the integral over substructure mass,  $M$ , from  $M_{min}$  to  $M_{max}$ , which we discuss below. We note that  $H[\xi_s(\Delta r, \Delta v)]$  also becomes a function of  $M$ .

Now we are able to calculate the dimensionless power spectrum  $\omega P_{\frac{\delta\nu}{\nu}}(\omega)$  in terms of the frequency  $\omega$  numerically, for Shapiro time delay and the Doppler effect. For convenience we define the dimensionless parameter  $h_p$  as

$$h_p \equiv [\frac{1}{2\pi} \omega P(\omega)]^{\frac{1}{2}}, \quad (37)$$

which is shown in Fig.(3) for the Doppler effect (solid line), Shapiro delay (dot-dashed line), and white noise (dashed line, which is computed in Appendix A). In order to calculate  $h_p$  numerically, we consider a realistic set of parameters (but later study the effect of changing these parameters). We choose the velocity of dark matter substructures  $v = 300 \text{ km/s}$  (typical of relative velocities in the Milky Way halo), the typical distance of pulsars to  $z_0 = 1 \text{ kpc}$ , the mean fraction of bound particles that can survive the tidal disruption period  $\mu = 0.03$  [12], the minimum mass of DM substructure  $M_{min} = 10^{-6} M_\odot$  and also the maximum  $M_{max} = 10^{12} M_\odot$  (the total mass of a galactic halo). Later we will show that  $h_p$  is almost independent of  $M_{max}$ .

The power spectra of Shapiro and Doppler effects in Fig.(3) are well described by power-laws:

$$\omega P_{\frac{\delta\nu}{\nu}}(\omega)|_{\text{Shapiro}} \propto \omega^{-3}, \quad \omega P_{\frac{\delta\nu}{\nu}}(\omega)|_{\text{Doppler}} \propto \omega^{-4}. \quad (38)$$

These behaviors can be understood by noticing that the  $\Delta v$  integral (*i.e.* the last integral) in Eqs. (35-36) scales

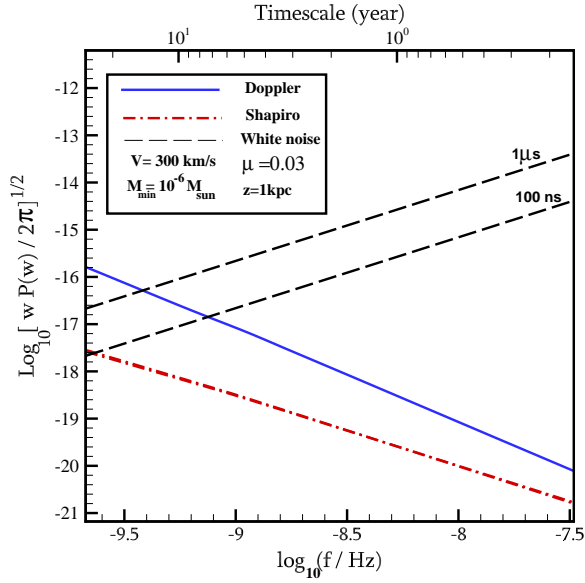


FIG. 3: Pulsar residual power spectrum as a function of frequency (bottom x-axis) and the span of observation time in years (top x-axis) for time delay caused by the Doppler effect (solid line) and time delay caused by Shapiro effect (dash-dot line). The long dashed lines represent levels of white noise for 100 ns (bottom) and 1  $\mu$ s (top) measured bi-weekly (see Appendix A) [13].

as  $H^2(\xi_s)$ , if we use the spherical collapse relations of Sec. (III). Since most small structures with CDM initial conditions collapse around the same time, this is approximately constant. The contribution to the rest of the integrals is dominated by  $k_y^{-1} \sim \Delta r \sim v/\omega$ , so the integral over distances scales as  $(\Delta r)^3 \propto \omega^{-3}$ . Plugging this into Eqs. (35-36) yields the scalings of Eq. (38).

To physically understand the scaling for the Doppler effect we can once more Fourier transform the power spectrum in Eq. (36) to find that  $v_{Dop.} \sim \frac{\delta v}{\nu}$  is proportional to  $vt^2 = (vt) \times t$ , i.e. the magnitude of acceleration is proportional to distance traveled by the earth/pulsar. This is exactly what one expects for the gravitational field in a medium with roughly uniform density, and is due to the fact that most small substructure forms at roughly the same density  $\propto H^2(\xi_s)$ . However, the direction of acceleration is random, as different substructures will dominate the local gravity on different scales.

An important point to consider before examining the effect of different parameters on pulsar timing is the study of the effect of maximum mass in the integrals. As we show in Fig. (4), the total dependence of  $h_p$  on maximum mass is small, where we plot the  $h_p$  for  $M_{max} = 10^{12} M_\odot$ , the total mass of a typical galaxy and  $M_{max} = 10^8 M_\odot$ , for a more realistic tidal cut-off for subhaloes at our position in the Milky Way. This confirms that, not surprisingly, most of the observable effects on

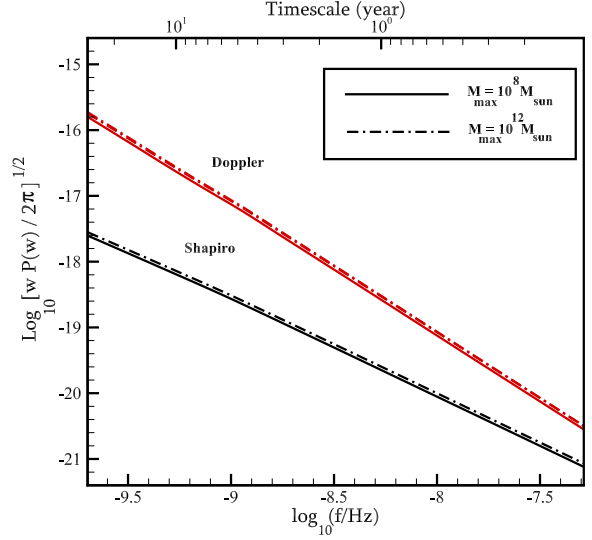


FIG. 4: Pulsar residual power spectrum as a function of frequency (bottom-x axis) and the span of time in years (top x-axis) for time delay caused by the Doppler effect (top-line) and time delay caused by Shapiro effect (bottom line) for a maximum mass of halo  $M_{max} = 10^{12} M_\odot$  (dash-dot line) and  $M_{max} = 10^8 M_\odot$  (solid line).

pulsar timing comes from CDM small scale structure.

Now we examine the dependence of the power spectrum on different parameters of the model. We plot the dimensionless amplitude  $h_p$  for the Doppler effect for different velocities of dark matter substructures and the  $\mu$ -parameter of stable clustering in Fig. (5), which shows that  $h_p$  is proportional to velocity and the square root of the  $\mu$  parameter.

In Fig. (6), we plot the power spectrum for different mass minima of DM substructures. As shown in Fig. (6), the  $\omega^{-4}$  dependence of  $h_p^2$  does not change by changing the minimum of the mass. However, the amplitude of the signal increases when the interval of integration is increased.

In Figs. (7) and (8) we plot  $h_p$  given different primordial spectral index  $n_s$ , for Doppler and Shapiro effects respectively. For  $n_s < 1$ , the slope of  $h_p$  does not change, as  $\sigma(M)$  becomes flat for low masses. On the other hand for larger  $n_s$ , we see a shallower  $\omega$  dependence for  $h_p$  as there is more power on small scales.

## V. OBSERVATIONAL PROSPECTS

Finally, to explore the observational prospects for the detection of pulsar frequency change due to dark matter substructures, we compare our results with the observational bounds put on detection of gravitational waves (GW) by pulsars. The observed quantities are similar in

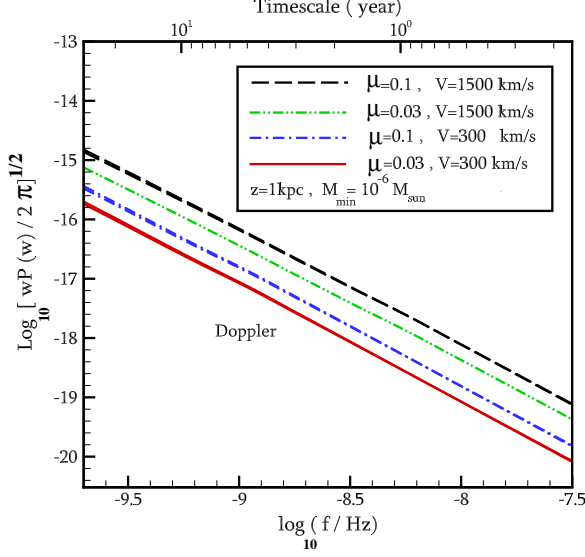


FIG. 5: Pulsar residual power spectrum as a function of frequency (bottom-x axis) and the span of time in years (top x-axis) for Doppler effect (solid line) for different velocities and  $\mu$  of dark matter substructures.

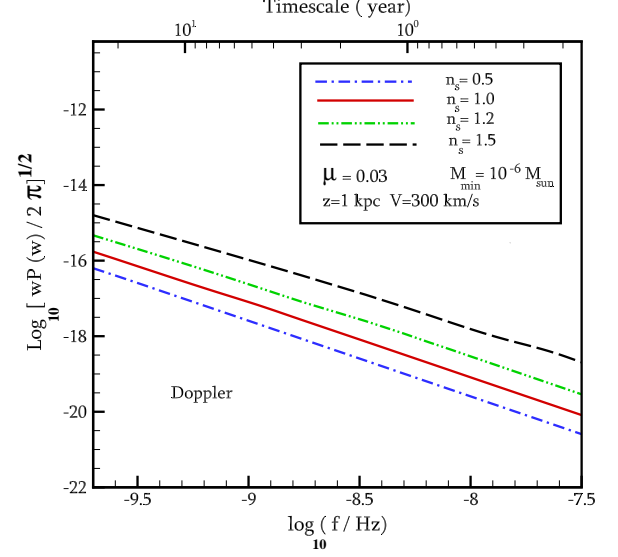


FIG. 7: Pulsar residual power spectrum as a function of frequency (bottom-x axis) and the span of time in years (top x-axis) for Doppler effect for different primordial index of matter power spectrum.

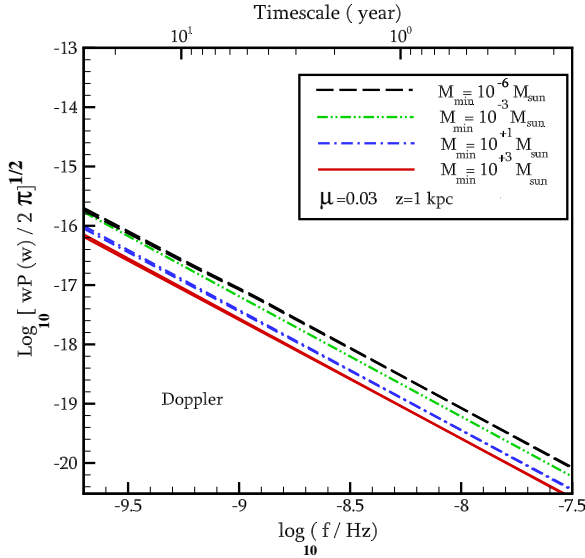


FIG. 6: Pulsar residual power spectrum as a function of frequency (bottom-x axis) and the span of time in years (top x-axis) for Doppler effect (solid line) for different minimum masses of dark matter substructures.

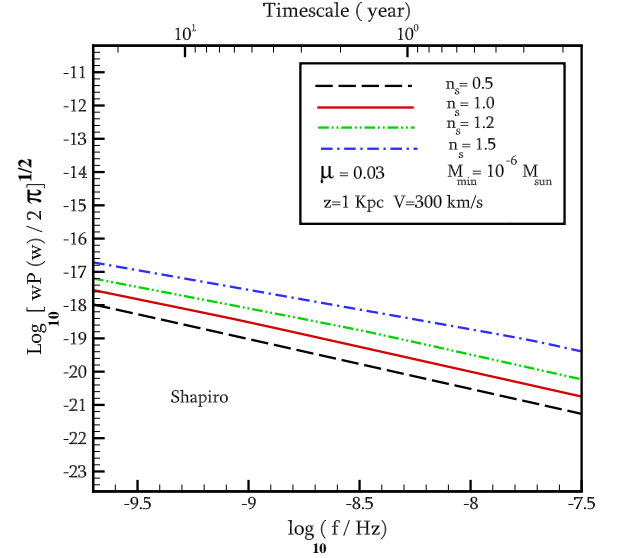


FIG. 8: Pulsar residual power spectrum as a function of frequency (bottom-x axis) and the span of time in years (top x-axis) for Shapiro effect for different primordial index of matter power spectrum.

both cases, and the power spectrum of pulsar frequency change caused by Doppler or Shapiro effects is red similar to gravitational waves. That is, there is an excess power at low frequencies, or long timescale correlations in residuals. The gravitational wave effect on pulsar timing is also in the  $n\text{Hz}$  frequency range [15, 21], similar to the substructure effect we are considering here.

In particular, the frequency change due to gravitational waves is roughly  $\sim h_{ij}$ , the amplitude of gravitational waves, which allows us to directly translate constraints on  $h_{ij}$ , to constraints on  $\delta\nu/\nu$ . Moreover, similar to the characteristic quadrupolar pattern that gravitational waves induce in pulsar timing residuals (*e.g.*, [21]), the Doppler effect induces a *dipolar* pattern in the sky,



which can be used to distinguish it from intrinsic changes in individual pulsars.

In Fig. (9) we plot the realistic and optimistic predictions for detection of  $h_p$ , which is similar to the gravitational wave dimensionless strain, and compare it with the current observational limits from a pulsar timing array [14] considering the sensitivity limit for time residuals of observed millisecond pulsars obtained via (see the appendix of [22] for details)

$$h_p^{lim} \propto \frac{\delta t_{rms} f}{N_p^{1/2} (T \Delta f)^{1/4}}, \quad (39)$$

where  $h_p^{lim}$  is the sensitivity limit of detectors,  $\delta t_{rms} = \sqrt{\langle \delta t^2 \rangle}$  is the root mean square value of the timing residuals,  $\Delta f$  is the frequency bandwidth of search,  $N_p$  is the number of pulsars and  $T$  is time span of observation. The Pulsar timing array sensitivity is scaled with frequency as  $h_p^{lim} \propto f$  and reaches a minimum at a detectable frequency of  $f \sim 1/T$ . This produces the wedge like sensitivity limit curves in Fig. (9). The sensitivity limit is also proportional to  $\delta t_{rms}$ , improving as the precision of pulsar timing residuals detection is increased. By increasing the observational time, we increase the sensitivity and also the span of frequency.

We also plot the predicted sensitivity of Parkers Pulsar Timing Array (PPTA) [23] and the Square Kilometer Array (SKA) [24] for  $h_p$ . The upper bounds for future PPTA and SKA experiments are obtained from the detectable time residual correlation of simulated pulsars with consideration of all instrumental, calibration and observational errors (such as pulsar intrinsic period changes and glitches)[25]. For example the PPTA bound is obtained by considering 20 radio pulsars for 5 year with  $\delta t_{rms} = 100ns$  which provides a peak sensitivity of  $h_p^{lim} \approx 2 \times 10^{-15}$  at  $f \approx 7 \times 10^{-9}$ . For SKA, with the same number of pulsars, the sensitivity is improved by increasing the span of observation to 10 years with timing accuracy  $\delta t_{rms} = 10ns$ , leading to a constraint on the pulsar residual power spectrum of  $\sim 1.6 \times 10^{-16}$  at  $f \approx 7 \times 10^{-9}$  [22].

Our results show that while current observations are unable to detect the effect of dark matter substructure on pulsar timing, error projections for the upcoming Square Kilometer Array (SKA) are only a factor of few higher than our optimistic predictions.

In the end, we should note that, unlike the Doppler effect, the Shapiro time delay does not have a coherent pattern on the sky, as different lines of sight are largely uncorrelated. This makes it much harder to distinguish Shapiro time delay from pulsar intrinsic frequency changes.

## VI. CONCLUSIONS AND DISCUSSION

In this work, we studied the gravitational effect of DM substructures on pulsar timing, through Doppler and

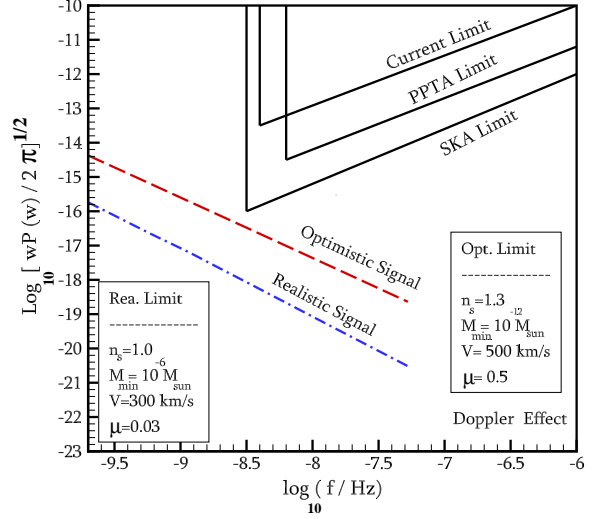


FIG. 9: Pulsar residual power spectrum as a function of the frequency for Doppler effect for realistic and optimistic signals (see text for definition of realistic and optimistic parameters). The limits from current and future experiments are also shown.

Shapiro (or ISW) effects. We calculated the dimensionless power spectrum of a pulsar's frequency change, which is related to the matter density power spectrum in the non-linear regime. We used the stable clustering hypothesis to extract the non-linear matter power spectrum, and showed that the frequency change is dominated by the Doppler effect. Next we varied the free parameters of the model, which had the following effects on the dimensionless power,  $h_p$ :

1.  $h_p$  due to Doppler effect is linearly proportional to velocity of DM substructures.
2. The main contribution of DM substructures comes from the minimum mass in DM hierarchy: as we increase the domain of integration over DM subhalo masses, we get more signal.
3.  $h_p$  has a dependence on  $\mu^{1/2}$ , the fraction of particle pairs that remain bound in the stable clustering hypothesis.
4.  $h_p$  due to the Shapiro effect scales as the square root of distances to pulsars, as it depends on the integrated gravitational effect over the line of sight.
5. For larger primordial spectral index,  $n_s$ , the frequency dependence of  $h_p$  is shallower, because the main contribution of  $h_p$  comes from low masses, where the power is increased. However, for  $n_s < 1$ , the frequency dependence becomes independent of  $n_s$ .

Finally, we compared the dimensionless power spectrum of pulsar frequency change, for realistic and optimistic sets of parameters, with current and future pulsar timing experiments, designed for detection of gravitational waves. Our results show that our optimistic estimate of the  $h_p$  signal is only a factor of a few smaller than the sensitivity of the planned Square Kilometer Array (SKA), making this method a potentially promising avenue for the detection of DM substructure on very small scales.

While our paper lays the groundwork for future statistical detection of dark matter substructure through pulsar timing, many practical challenges and theoretical uncertainties remain. Here we point out two, along with potential resolutions:

First, it is important to note that the observed Doppler effect in pulsar timing depends on the total gravitational acceleration, which can be contributed by nearby stars/planets, in addition to local dark matter substructure. However, the gravitational pull of stars/planets on earth can be calculated by knowing their masses and positions around earth, and thus, in principle, can be computed and corrected for. Similar effects on the acceleration of pulsars will be uncorrelated for different pulsars, and thus can be distinguished from earth's acceleration.

A second concern is the possible non-gaussianity of the signal. For example, microlensing events due to stars in the Galactic halo could lead to large magnifications, but have very small optical depth, and thus happen rarely. Therefore, the power spectrum gives a very incomplete description of the observables in microlensing events. However, in contrast to magnification events that trace projected density, the gravitational effects on pulsar timing that we discuss here trace the integrated potential, which is much more smooth. Moreover, the small CDM substructure are much more diffuse than stars, which further reduces the skewness of the signal. Therefore, unlike microlensing events, the observed signal is likely to be contributed by a variety of structures on different scales (*e.g.* Fig. 6) with no sharp boundaries. This is why we expect a close to gaussian signal, simply based on central limit theorem, which suggests that the power spectrum might provide adequate statistical description of these effects.

### Acknowledgments

We would like to thank Sohrab Rahvar, Adrienne Erickcek and Ethan Siegal for discussion and valuable comments. SB thanks the Perimeter Institute for their kind hospitality during a visit where part of this work began. NA is supported by Perimeter Institute (PI) for Theoretical Physics and Natural Sciences and Engineering Research Council of Canada (NSERC). Research at PI is supported by the Government of Canada through Indus-

try Canada and by the Province of Ontario through the Ministry of Research & Innovation.

### Appendix A: Statistics of $\sigma_z$ for stability of Pulsars and White noise calculation

The ability of a pulsar timing array to detect any delay in the received pulses to measure the dark matter halos substructures depends on the pulsar timing stability. Timing stability is related to how long the rms of timing residuals can be kept small, from which we can estimate the potential to detect Doppler and Shapiro effects. Statistical artifacts such as a large gap in data sampling, or a large variation in error-bar size, may prevent a reliable power spectrum of pulsar timing data. An alternative approach is  $\sigma_z$  statistics, as described by *e.g.* Matsakis et al. [26]:

$$\sigma_z(\tau) = \frac{\tau^2}{2\sqrt{5}} \langle c_3^2 \rangle^{1/2}, \quad (\text{A1})$$

where  $\langle \rangle$  denotes the average over subsets of the pulsar timing data, and  $c_3$  is determined from a polynomial fit

$$c_0 + c_1(t - t_0) + c_2(t - t_0)^2 + c_3(t - t_0)^3 \quad (\text{A2})$$

to timing residuals for each subset, and  $\tau$  is the length of the subsets. In order to connect our theoretical calculations to the observed pulsar time residuals we should find a relation between  $\sigma_z$  and the calculated power spectrum. From the polynomial fit to the timing residuals we find that

$$c_3 \simeq \frac{1}{6} \frac{d}{d\tau} \Delta \ddot{t} |_s \simeq \frac{1}{6} \frac{d}{d\tau} \frac{\dot{\delta\nu}}{\nu}, \quad (\text{A3})$$

where we assume that the fitting procedure depends on  $\Delta t |_s$ , which is coarse grained on the scale of  $\tau$ . The correlation function  $c_3$  can be written as

$$\langle c_3^2 \rangle = \frac{1}{18} \{ \langle (\frac{\dot{\delta\nu}}{\nu})^2 \rangle - \langle (\frac{\dot{\delta\nu}}{\nu})|_1 (\frac{\dot{\delta\nu}}{\nu})|_n \rangle \}. \quad (\text{A4})$$

Now, using Eqs.(9,A1,A4) we obtain

$$\sigma_z(\tau) \simeq \frac{\tau}{6\sqrt{5}} \left\{ \int_0^{\frac{1}{\tau}} \frac{d\omega}{2\pi} \omega^2 P(\omega) [1 - \cos(\omega\tau)] \right\}^{1/2}. \quad (\text{A5})$$

In order to find the white noise corresponding to pulsar timing we derive the relation of the dimensionless power spectrum of pulsars with the sampling time and the uncertainty in the pulsar timing measurement. The cross correlation of time residuals of pulsar timing is related to the accuracy of measurement  $t_a$  as

$$\langle \delta t(t_1) \delta t(t_2) \rangle = (t_a)^2 \delta_{t_1 t_2}, \quad (\text{A6})$$

where  $\delta_{t_1 t_2}$  is Kronecker delta and  $\delta t$  is the time residual of pulsar timing related to frequency change as

$$\delta t = \int \frac{\delta \nu}{\nu} dt \quad (\text{A7})$$

The correlation of timing residuals can be approximated in the time span of  $\tau$ , which is the period of sampling as:

$$\langle \delta t(t_1) \delta t(t_2) \rangle \simeq (t_a)^2 \tau \delta(t_1 - t_2) \quad (\text{A8})$$

Now the power spectrum of time residuals is obtained as

$$P_{\delta t}(\omega) = \int e^{-i\omega t} \langle \delta t(t_1) \delta t(t_2) \rangle dt = \tau t_a^2, \quad (\text{A9})$$

which yields the dimensionless power spectrum,

$$h_p = \left[ \frac{1}{2\pi} \omega P_{\delta t}(\omega) \right]^{1/2} = \frac{\sqrt{\tau}}{\sqrt{2\pi}} \omega^{3/2} t_a. \quad (\text{A10})$$

To find the white noise lines in Fig.(3), we set the sampling time of pulsar timing  $\tau$  to be 2 weeks and the accuracy of pulsar timing,  $t_a$ , to be 100ns and 1 $\mu$ s.

- 
- [1] N. Jarosik *et al.*, arXiv:1001.4744 (2010).
  - [2] M. Roos, Dark Matter: The evidence from astronomy, astrophysics and cosmology. arXiv:1001.0316 (2010).
  - [3] A. Loeb and M. Zaldarriaga, Phys. Rev. D **71**, 103520 (2005); S. Profumo, K. Sigurdson and M. Kamionkowski, Phys. Rev. Lett. **97**, 031301 (2006).
  - [4] . D.A. Frail *et al.*, Astrophysical J., Vol. 1, **436**, no.1, 144 (1994).
  - [5] I.I. Shapiro, Phys. Rev. Letters **13**, 789 (1964).
  - [6] E.R. Siegel, M.P. Hertzberg and J.N. Fry, MNRAS, 382, Issue 2, 879 (2007).
  - [7] T.I. Larchenkova and S.M. Kopeikin, Astronomy Letters, Vol. 32, **1**, 18 (2006).
  - [8] A. Erickcek and N.M. Law, arXiv: 1007.4228 (2010).
  - [9] M. Davis and P.J.E. Peebles, ApJS **34**, 425 (1977).
  - [10] A.J.S. Hamilton, A. Matthews, P. Kumar and E. Lu, Astrophys. J. **374**, L1 (1991); B. Jain, H.J. Mo and S.D.M. White, Mon. Not. Roy. Astron. Soc. **276**, L25 (1995).
  - [11] J.A. Peacock and S.J. Dodds, Mon. Not. Roy. Astron. Soc. **280**, L19 (1996).
  - [12] N. Afshordi, R. Mohayaee and E. Bertschinger, Phys. Rev. D **81**, 101301 (2010).
  - [13] J.P.W. Verbiest *et al.*, MNARS, Volume 400, Issue 2, 951 (2009).
  - [14] F.A. Jenet *et al.*, ApJ. **653**, 1571 (2006).
  - [15] F.A. Jenet, G.B. Hobbs, K.J. Lee and R.N. Manchester, Astrophys. J. **625**, 123 (2005).
  - [16] R.K. Sachs, and A.M. Wolfe, Astrophys. J. 147, 73 (1967).
  - [17] J.E. Gunn and J.R. Gott, Astrophys. J. **176**, 1 (1972).
  - [18] J.M. Bardeen, J.R. Bond, N. Kaiser and A.S. Szalay, ApJ, **304**, 15 (1986).
  - [19] A. Cooray and R.K. Sheth, Phys. Rept. **372**, 1 (2002).
  - [20] R.E. Smith *et al.*, MNRAS, Volume 341, Issue 4, 1311 (2003).
  - [21] G. Hobbs, F.A. Jenet, K.J. Lee, J.P.W. Verbiest, D. Yardley, R. Manchester, A. Lommen, W. Coles, R. Edwards and C. Shettigara, MNRAS, **394**, 1945 (2009).
  - [22] A. Sesana, A. Vecchio and C.N. Colacino, MNARS, **390**, 192 (2008).
  - [23] R. N. Manchester, arXiv: 1004.3602 (2010); G.B. Hobbs *et al.*, PASA **26**, 103 (2009); J.P.W. Verbiest, *et al.*, Class. and Quant. Grav. **27**(8), 084, 015 (2010).
  - [24] R. Smiths, *et al.*, Pulsar searches and timing with SKA, arXiv:0811.0211 (2008).
  - [25] G. Hobbs, Pulsars as Gravitational Wave detectors, arXiv: 1006.3969 (2010).
  - [26] D.N. Matsakis, J.H. Taylor and T.M. Eubanks, AA, **326**, 924 (1997).